

Impact of the molecular quadrupole moment on ionization energy and electron affinity of organic thin films: Experimental determination of electrostatic potential and electronic polarization energies

Kazuto Yamada,^{1,*} Susumu Yanagisawa,² Tomoyuki Koganezawa,³ Kazuhiko Mase,^{4,5} Naoki Sato,¹ and Hiroyuki Yoshida^{6,7,†}

¹*Institute for Chemical Research, Kyoto University, Gokasho, Uji, Kyoto 611-0011, Japan*

²*Department of Physics and Earth Sciences, Faculty of Science, University of the Ryukyus, 1 Senbaru, Nishihara, Okinawa 903-0213, Japan*

³*Japan Synchrotron Radiation Research Institute (JASRI), SPring-8, 1-1-1 Kouto, Sayo, Hyogo 679-5198, Japan*

⁴*Institute of Materials Structure Science, High Energy Accelerator Research Organization (KEK), 1-1 Oho, Tsukuba, Ibaraki 305-0801, Japan*

⁵*School of High Energy Accelerator Science, SOKENDAI (The Graduate University for Advanced Studies), 1-1 Oho, Tsukuba 305-0801, Japan*

⁶*Graduate School of Engineering, Chiba University, 1-33 Yayoi-cho, Inage-ku, Chiba 263-8522, Japan*

⁷*Molecular Chirality Research Center, Chiba University, 1-33 Yayoi-cho, Inage-ku, Chiba 263-8522, Japan*



(Received 8 March 2018; published 20 June 2018)

Energy levels of organic molecular films exert paramount influence on the electronic properties of organic semiconductors. Recently the effect of electrostatic energy was highlighted as an origin of such peculiar phenomena as the molecular-orientation dependence and continuous tuning of energy levels. However, the mechanism has been discussed mostly based on theoretical work and has not been adequately supported by experiments. In this work, we propose a procedure to evaluate the electrostatic and electronic polarization energies in organic films solely from the experimental data obtained by ultraviolet photoelectron and low-energy inverse photoelectron spectroscopies. We apply it to the energy levels of thin films of 6,13-pentacenequinone on SiO₂ substrates with three different molecular orientations. The obtained electrostatic energies are fully consistent with the theoretical results at different levels such as the first-principles calculations and the electrostatic energy of charge-multipole interactions. The present work also underlines the importance of the charge-permanent quadrupole interaction which is the leading term of the electrostatic energy in the film of nonpolar molecules.

DOI: [10.1103/PhysRevB.97.245206](https://doi.org/10.1103/PhysRevB.97.245206)

I. INTRODUCTION

Understanding the factors that determine the energy levels of organic solids is of great importance to the research and development of organic semiconductor devices, e.g., organic light emitting diodes, organic photovoltaic cells, and organic transistors [1,2]. The organic solid is an aggregate of molecules bound by weak intermolecular interactions such as dispersion and electrostatic forces, while the constituent molecules consist of atoms bound by covalent bonds. As the intermolecular interactions are usually one order of magnitude smaller than the intramolecular ones, the energy levels of an organic solid can be regarded as the electronic levels of an isolated molecule perturbed by weak intermolecular interactions due to the classical and quantum effects [3]. The classical effect is dominated by the polarization energy which is the interaction between the localized charge carrier and neutral surrounding molecules [4]. The magnitude is in the range between 1 eV (1 eV \approx 1.602 \times 10⁻¹⁹ J) and 2 eV [5]. On the other hand, the quantum effect can be observed as the band dispersion. The bandwidth is usually less than 0.1 eV in common organic semiconductors, while that of organic solids with high carrier mobility exceeds 0.4 eV [6–11].

The energy levels of organic solids are represented by the ionization energy I_s and electron affinity A_s corresponding to the edges of hole and electron conduction levels with reference to the vacuum level, respectively. In the previous work [12], we proposed the I_s and A_s expressed in connection with the ionization energy I_g and electron affinity A_g in the gas phase, respectively, as

$$\begin{aligned} I_s &= I_g - P^+ - \Delta^+, \\ A_s &= A_g + P^- + \Delta^-, \end{aligned} \quad (1)$$

where the contribution from the polarization energies for positive P^+ and negative P^- charges and the effect of bandwidths of the highest occupied molecular orbital (HOMO) and lowest unoccupied molecular orbital (LUMO) derived bands, Δ^+ and Δ^- , respectively, are taken into account. This is a modification of the well-known relation by Lyons [4]. Although the polarization energy includes contributions from molecular and lattice relaxations, they are smaller than 0.1 eV [13]. Only the electronic effects are discussed here.

The polarization energy P^+ and P^- can further be divided into two terms, the electrostatic energy W and electronic polarization energy E_p [14–18]. The latter is also referred to the induction contribution [17] or dynamic interaction [18]. The E_p is an induced effect that minimizes the total energy and approximated by the charge-induced dipole interaction. In contrast, the electrostatic energy W is the interaction between the excess charge and the molecular charge (charge distributed

*Present address: Department of Chemistry, Graduate School of Science, Kyoto University, Kyoto 606-8502, Japan.

†hyoshida@chiba-u.jp

over the neutral molecules) and is approximated by the charge-permanent multipole interaction.

The electronic polarization interaction is short range and isotropic. Further, its magnitude does not strongly depend on the materials [5]. As far as the electronic polarization is concerned, the energy levels of an organic solid can be estimated from those of its constituent single molecule. Based on this assumption, the ionization energy I_s and electron affinity A_s are routinely estimated using the cyclic voltammetry or the density functional theory (DFT) calculation for an isolated molecule.

On the other hand, the electrostatic interaction is long range and highly anisotropic. It has been highlighted recently as the origin of the orientation dependence of the energy levels in molecular films [19,20] and continuous tuning of the energy levels by mixing two molecules having permanent quadrupole moments with opposite direction [21,22]. Further, theoretical studies have pointed out that the energy level may also depend on the macroscopic shape of the sample [16,17,23]. Such electrostatic interaction can play an important role in the charge separation in organic photovoltaic cells [24–26].

Among the above examples, the orientation dependence of the energy levels has been most intensively discussed so far. The orientation dependences of ionization energies have been observed for many organic solids using ultraviolet photoelectron spectroscopy (UPS) [19,27–36]. The origin is proposed to be the electrostatic potential generated by the permanent quadrupole moment of molecules. This argument has been supported by good agreement between the experimental data and theoretical predictions [12,16,20]. The opposite orientation dependence of energy level was observed for similar molecules with opposite quadrupole moment (e.g., copper phthalocyanine and copper hexadecafluorophthalocyanine [27], pentacene and perfluoropentacene [28]) providing a further support. This phenomenon has been applied to modification of the work function [37] and optoelectronic devices [38]. In any case, however, the mechanism of the orientation-dependent energy levels are mainly discussed based on the theoretical consideration and the experimental data have provided only indirect evidence. More specifically, the quantitative values of the electrostatic potential have never been evaluated from experimental data alone.

Recently, we developed low-energy inverse photoelectron spectroscopy (LEIPS) [39–41] demonstrating that electron affinities of various organic materials can be determined with precision similar to that of the ionization energy by UPS [42–50]. Based on the precisely determined electron affinity together with the ionization energy, we precisely determined the increase of electronic polarization energy upon the crystallization of the 6,6-phenyl C₆₁-butyric acid methyl ester (PCBM) films [51]. Extending this idea, we anticipate determining the W and E_p solely from the experimental data.

In this work, we first propose a procedure to determine the electronic polarization and electrostatic energies from the experimental data, bearing the situation described above in mind. Then this method is effectually applied to the study of the molecular-orientation dependence of energy levels of 6,13-pentacenequinone [also called 6,13-pentacenedione (PNQ), C₂₂H₁₂O₂] films. In the earlier studies, the molecular-orientation dependence of ionization energies was examined

only roughly for standing and lying orientations [12,19,27–36]. Further, the molecular orientations are controlled by preparing the films on different substrates, e.g., the naturally oxidized surface of Si wafer (SiO₂) and highly oriented pyrolytic graphite (HOPG). The effect of different substrates cannot be neglected. We pay special attention to (1) quantitatively controlling the molecular orientation and the direction of molecular quadrupole and (2) preparing the film on the same kind of substrates to minimize the effects of the substrate. The obtained data will be able to be compared quantitatively with calculated results with different levels of theory. Here, we perform the first-principles calculations using DFT and the G_0W_0 approximation to calculate the electrostatic and electronic polarization energies, respectively. We also calculate the electrostatic energy of charge-multipole interaction to draw the potential maps and to examine the relation between the energy levels and the macroscopic shape of the sample.

II. THEORY

As mentioned above, the polarization energies, P^+ and P^- , can be expressed as the sum of the electronic polarization energy, E_p^+ and E_p^- , and the electrostatic energy, W^+ and W^- , respectively, for positive and negative ions,

$$\begin{aligned} P^+ &= E_p^+ + W^+, \\ P^- &= E_p^- + W^-. \end{aligned} \quad (2)$$

As Topham and Soos pointed out, the polarization energy may contain a cross term between the electronic polarization energy and the electrostatic energy [16]. Since the cross term is a few tenths of an eV, we neglect it. The electronic polarization E_p is proportional to the square of the excess charge and the value does not depend on the sign of the charge. Thus the electronic polarization energies for positive E_p^+ and negative E_p^- charges are approximated to be the same, $E_p \equiv E_p^+ = E_p^-$. In contrast, the electrostatic energy W is a linear function of the excess charge and the sign of W depends on the polarity of the excess charge. The electrostatic energies for positive W^+ and negative W^- charges are approximately the same in the magnitude but of opposite sign, $W \equiv W^+ = -W^-$. Inserting these relations into Eq. (2) yields

$$\begin{aligned} E_p &= (P^+ + P^-)/2, \\ W &= (P^+ - P^-)/2. \end{aligned} \quad (3)$$

Note the above relation holds rigorously when the multipole expansion is applied [15]. In practice, E_p^+ and E_p^- , and also W^+ and $-W^-$, may not be exactly the same because the charge distributions are not always the same between the cation and anion of the same molecule.

III. EXPERIMENT

We purchased PNQ and pentacene from Aldrich and purified by cycles of vacuum sublimation before use. Silicon substrates with native oxide surface (SiO₂) were sonicated in acetone and ultrapure water, followed by heating to 700 K in vacuum for 2 h. PNQ or pentacene was vacuum deposited at the rate of 0.1–0.5 nm min⁻¹ under the vacuum of 5×10^{-7} Pa. A SiO₂ substrate covered with a single layer of graphene (Graphene Platform Corporation) was heated at 700 K for 24 h in order to remove polymer residues [52].

The polymorphs and molecular orientations were examined by grazing-incidence x-ray diffraction (GIXD), near-edge x-ray absorption fine structure (NEXAFS), and Fourier transform infrared spectroscopy (FTIR). The GIXD measurements were carried out at the beam line BL46XU of SPring-8. An x ray with a wavelength of 0.1 nm was incident to the sample surface with an angle of 0.06° – 0.16° and diffraction was observed using a two-dimensional (2D) detector (PILATUS 300K). NEXAFS in the O K -edge region was recorded in a total electron yield mode at the BL-13B of the Photon Factory (KEK-PF). FTIR was measured on a Thermo Scientific Nicolet iS10.

UPS and LEIPS were performed in separate apparatuses without air exposure of the samples. UPS spectra were measured with a He discharge lamp ($h\nu = 21.22$ eV) and a SPECS Phoibos 150 electron energy analyzer. The vacuum level was determined from the cutoff energy for the secondary electron region in an obtained spectrum. Details of the LEIPS apparatus are described elsewhere [53]. The measurements were carried out at photon energies of 3.71, 4.13, and 4.89 eV. The vacuum level was determined as the inflection point of the rising edge of the sample current. No discernible change due to the sample damage was observed during the LEIPS measurements.

IV. RESULTS

We employ PNQ because it has a large quadrupole moment along the molecular long axis. The charge distribution in PNQ, as shown by the electrostatic potential map in Fig. 1(a), calculated at the B3LYP/6-31G(*d*) level [54] can be approximated by a quadrupole moment along the molecular long axis [55]. Thus it is essential to discuss the angle of the molecular long axis with respect to the substrate surface. For the substrate, we adopt SiO_2 because it has a chemically inert surface as well as sufficient conductivity for the electron spectroscopies, flat surface for grazing-incidence x-ray diffraction (GIXD), and transparency in the infrared region for Fourier transform infrared spectroscopy (FTIR) (see the Supplemental Material [56]).

Fabricating organic films with controlled molecular orientations is challenging. The PNQ film shows two polymorphs with standing molecular orientation on SiO_2 [57–60]: a monoclinic structure ($P2_1/b$) and a triclinic structure ($P\bar{1}$) in which the molecular long axes tilt by 55° and 33° from the normal to the substrate surface, respectively [60]. Thus thin films with at least two different molecular orientations can be prepared when the polymorphs are controlled. While the monoclinic form grows on the SiO_2 surface normally, it is reported that the triclinic form of PNQ is exclusively observed when pentacene and PNQ are codeposited [59]. Inspired by this, we inserted a monolayer of pentacene between SiO_2 and PNQ for preferential growth of the triclinic form. On the other hand, PNQ is expected to show a lying orientation on HOPG and graphene as is usually observed for polyacene molecules, e.g., pentacene [8,52,61,62] and perfluoropentacene [63,64].

Figure 1(b) shows GIXD patterns of the differently prepared PNQ films in the thickness of 5 nm. The PNQ film on graphene/ SiO_2 shows the (0 2 0), (0 4 0), and (0 6 0) diffractions of the monoclinic form (M) tilted by 40° from the surface normal, signifying that the molecules take a lying-flat orientation with the [1 4 0] axis normal to the substrate surface. A similar diffraction pattern was observed for PNQ on HOPG

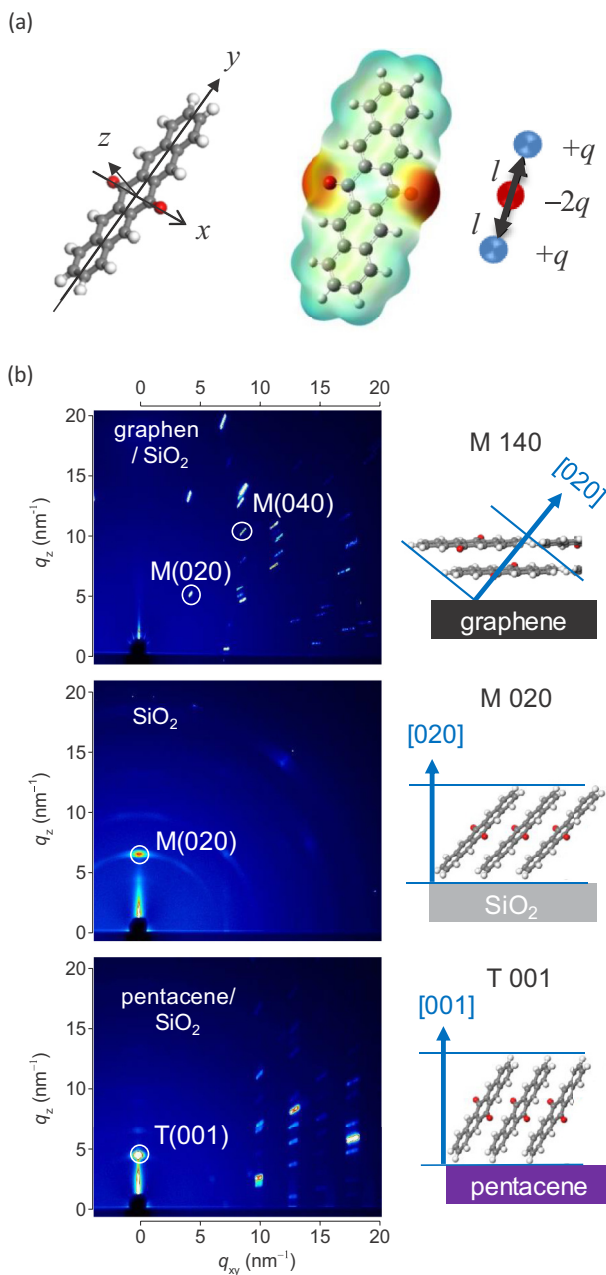


FIG. 1. (a) The molecular structure and definition of the molecular axes (left). The electrostatic potential map (right) can be modeled by a permanent quadrupole with three point charges lying on a straight line along the molecular long axis (see text). (b) The grazing incidence x-ray diffraction patterns of the PNQ films in the thickness of 5 nm on the single-layer graphene/ SiO_2 , pristine SiO_2 , and monolayer pentacene/ SiO_2 . M and T denote the monoclinic and triclinic forms, respectively. The determined molecular orientations are schematically shown alongside the diffraction patterns. The detailed information about the molecular orientations is given in Table I.

(Fig. S3, Supplemental Material [56]) showing that the films on the graphene and HOPG are the same in the crystallographic structure and molecular orientation [56]. On the pristine SiO_2 , the (0 2 0) diffraction of the monoclinic form (M) was observed normal to the substrate surface. The triclinic structure (T) was observed on pentacene/ SiO_2 with the (0 0 1) diffraction along

TABLE I. Crystal system and molecular orientation of PNQ films determined by GIXD and NEXAFS (Fig. 1). The angles of molecular short-axis θ_x , long-axis θ_y , and normal to the plane θ_z are taken with respect to the surface normal of the substrate.

Substrate	Crystal system	Orientation	GIXD			NEXAFS
			θ_x (deg)	θ_y (deg)	θ_z (deg)	θ_z (deg)
Graphene/SiO ₂	Monoclinic	1 4 0	80.4	89.9	9.6	19
SiO ₂	Monoclinic	0 2 0	64.7	55.1	45.6	57
Pentacene/SiO ₂	Triclinic	0 0 1	67.4	33.0	67.3	69

the normal to the substrate. The determined polymorphs and orientations are summarized in Table I.

The orientations are further examined by oxygen *K*-edge spectra from NEXAFS (Fig. S1 [56]). The observed angle dependence of the peak intensities shows the angles of the molecular planes with reference to the normal of the surface are $\theta_z = 19^\circ$ on graphene/SiO₂, 57° on SiO₂, and 69° on pentacene/SiO₂. These results are in essentially good agreement with the x-ray diffraction results as shown in Table I. The slight differences between GIXD and NEXAFS data are due to the fact that the x-ray diffraction examines only the crystalline area while the NEXAFS examines both the crystalline and amorphous areas in the film. Actually, $\theta_z = 9^\circ$ for PNQ on HOPG (Fig. S3: panels (c,d) [56]) is in excellent agreement with 9.6° of the XRD result [56], suggesting that the PNQ film on graphene is less perfect than that on HOPG. We also assessed the purity of the polymorph by observing the C-C in-plane vibrational mode using FTIR [60]. The spectra in Fig. S2 clearly confirm the high purity of each polymorph in the prepared PNQ films [56]. Thus we will employ the angles determined by x-ray diffraction to represent the molecular orientations for further discussion.

Now that the PNQ films with the controlled molecular orientations were obtained, we carried out UPS and LEIPS measurements to determine their ionization energies and electron affinities. We confirmed that the spectra are independent of the film thickness between 5 and 15 nm (Fig. S6, Supplemental Material [56]). The electron affinities are determined from the data taken systematically at the different photon energies (Figs. S4 and S5 [56]). Figure 2 shows the combined UPS and LEIPS spectra of 15-nm-thick PNQ films. The ionization energies and electron affinities are determined from the onset of spectra which are considered to be the values corresponding to the bulk material rather than the surface [65–68]. We found that the ionization energy I and electron affinity A vary by 0.7 and 1.0 eV, respectively, depending on the molecular orientation while the band gap ($I-A$) is almost independent of the orientation ranging from 3.53 to 3.78 eV. The work function of the films which is the energy of the vacuum level E_{vac} of PNQ films with respect to the Fermi level E_F are about 4.5 eV and little depends on the molecular orientation.

V. DISCUSSION

From the determined energy parameters, I_s and A_s , of the film, we evaluate the polarization energies for positive and negative charges, P^+ and P^- , respectively, according to Eq. (1) [12]. For the energy parameters in the gas phase, we use the values of $I_g = 7.89$ eV and $A_g = 1.54$ eV calculated by

HSE06/6-311 + +G** [69] since the calculation was found to be sufficiently reliable [12]. Actually the calculated A_g is in close agreement with the experimental value determined by negative ion photoelectron spectroscopy (the adiabatic electron affinity of 1.43 ± 0.13 eV and vertical detachment energy of 1.55 ± 0.02 eV) [70]. The electron affinity in Ref. [69] is calculated for the neutral molecular structure and does not take the structural relaxation into account. The values is the vertical electron affinity and should be similar to the vertical detachment energy if the reorganization energies are the same between the anion and neutral molecules. On the other hand, the experimental value of electron affinity for the film is determined from the spectral onset of LEIPS; we can assume

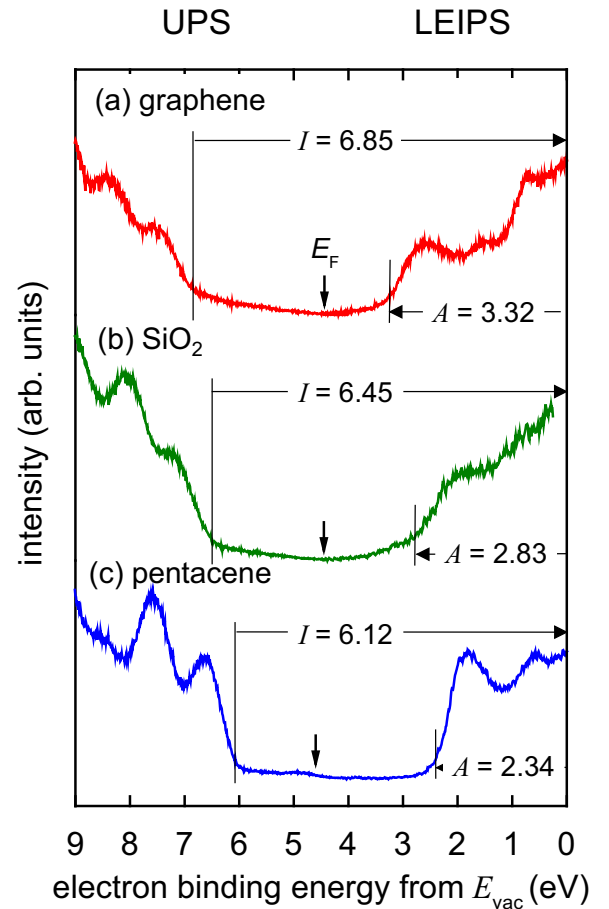


FIG. 2. The combined UPS and LEIPS spectra for the PNQ films in the thickness of 15 nm deposited on (a) single-layer graphene/SiO₂, (b) SiO₂, and (c) monolayer pentacene/SiO₂. The vertical arrows show positions of the Fermi level E_F .

TABLE II. Summary of electrostatic W and electronic polarization E_p energies for the PNQ film with different molecular orientations. The experimental values are obtained according to Eq. (2) based on the ionization energies and electron affinities while the theoretical W^\pm and E_p are by DFT calculation, and the many-body perturbation theory within the G_0W_0 approximation, respectively.

Structure		Experiment		First-principles calculation		
Molecular orientation	Surface	W (eV)	E_p (eV)	W^+ (eV)	W^- (eV)	E_p (eV)
90°	$M(140)$	-0.42	1.12	-0.21	0.41	1.08
55°	$M(020)$	0.03	1.07	0.25	-0.15	1.13
33°	$T(001)$	0.55	0.92	0.70	-0.63	1.18

it as an adiabatic electron affinity of the film. In any case, the relaxation is of the order of 0.1 eV and within the experimental uncertainties.

The energy contributions from the band widths in Eq. (1), Δ^+ and Δ^- , are approximated as half of the bandwidths obtained by the DFT calculation with the PW91 exchange-correlation functional [60]: $\Delta^+ = 0.34$ eV and $\Delta^- = 0.25$ eV for the monoclinic form, and $\Delta^+ = 0.30$ eV and $\Delta^- = 0.43$ eV for the triclinic form. Such simplification is acceptable because the variation in the bandwidth (0.49–0.86 eV) is small, and the difference between the Δ^+ and Δ^- values is essential in the following discussion. The above procedure and the evaluated polarization energies are shown in Fig. 3.

From the polarization energies, the electrostatic W and electronic polarization E_p energies are derived according to Eq. (3) as summarized in Table II. The electronic polarization energy E_p is in the range between 0.9 and 1.1 eV and almost independent of the molecular orientation. The electrostatic energy W , on the other hand, varies from -0.4 to +0.5 eV predominantly contributing to the orientation dependence of the polarization energy.

Since we have experimentally obtained the quantitative values for the electrostatic W and electronic polarization E_p energies, we compare them with calculated values at various theoretical levels. First, we performed the first-principles calculations. The electrostatic energy can be calculated based on DFT calculation. Details of the method are described in the Supplemental Material [56]. Here, the electrostatic contribution in the polarization energy, W^+ (or W^-), depending on the molecular orientation is approximated by the difference in

the HOMO (or the LUMO energy) between a 1-monolayer slab and an isolated molecule. The approximation may be validated by the “nearsightedness” of the quantum mechanical effects: Perturbation of the external potential at a region separated from a given location by larger than a typical de Broglie wavelength has a small effect upon any static property of a many-particle system at that location [71,72]. In other words, there is similarity in a local chemical environment, i.e., intramolecular chemical interaction, between a single molecule and a freestanding monolayer. On the other hand, the different electrostatic properties in a monolayer and in the gas phase were discussed [72]. The electronic polarization energy E_p is obtained by the many-body perturbation theory within the G_0W_0 approximation for the bulk system [73–76]. Further, the result is calculated as the narrowing of the band gap; we evaluated the average value E_p for positive and negative charges assuming $E_p^+ = E_p^-$. The results are compared with the experimental data in Table II.

The electrostatic energies W^+ and W^- are calculated for the 1-monolayer slab and may not be directly compared with the experimental value for the thick film. Nevertheless, the values agree well with each other. As we assumed in Eq. (2), the magnitude of the electrostatic energy for the positive W^+ and negative W^- charges are almost the same. The difference of about 0.1 eV is due to the differences in the charge distribution between the cation and anion as well as the different molecular polarizability to negative and positive charges. As mentioned before, the experimentally obtained electronic polarization energies E_p correspond to the bulk value rather than the surface value; this can be compared with E_p calculated by the G_0W_0 approximation for the bulk. Again the agreements are reasonable. These results suggest that the procedure represented by Eq. (2) gives us the W and E_p values from the experiment within the uncertainties of 0.1 eV.

When the multipole expansion is applied, the leading term of the electronic polarization energy is the charge-induced dipole interaction in the case of nonpolar molecules. In order to further explore the effect of the electrostatic energy, we calculate the electrostatic potential formed by permanent quadrupoles located at the molecular positions within a disk cluster of thickness t and diameter d . The potential energy is calculated by $U = e/(4\pi\epsilon_0r^5) \sum^t \mathbf{r}\mathbf{Q}\mathbf{r}$, where e and ϵ_0 are the elementary charge and the permittivity of vacuum, respectively, and the sum runs over the center-of-mass positions of the neutral molecules \mathbf{r} with respect to the charge. The quadrupole tensor \mathbf{Q} was calculated at the B3LYP/6-311 + G(d, p) level [77]. Figure 4(a) shows the potential maps for the clusters of $t = 4$ nm and $d = 20$ nm. The calculated potential inside the cluster is almost uniform and depends on the molecular orientation, 1.0, 0.4, and -2.1 eV for $\theta_y = 90^\circ$

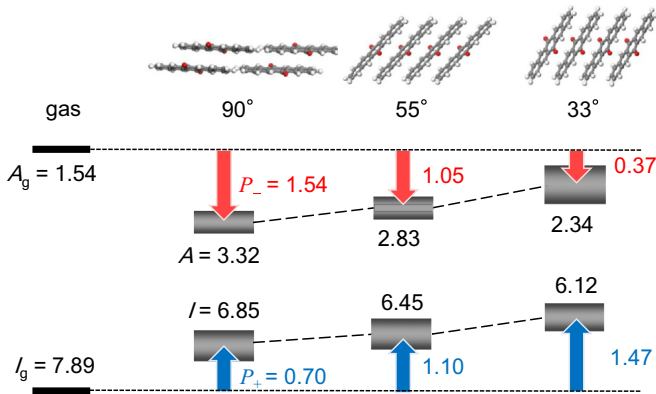


FIG. 3. The energy parameters (in eV) obtained by the UPS and LEIPS measurements for the different molecular orientations with indicated molecular tilt angles. The polarization energies for positive P^+ and negative P^- charges calculated according to Eq. (1). The height of a gray block indicates the bandwidth $2\Delta^+$ or $2\Delta^-$.

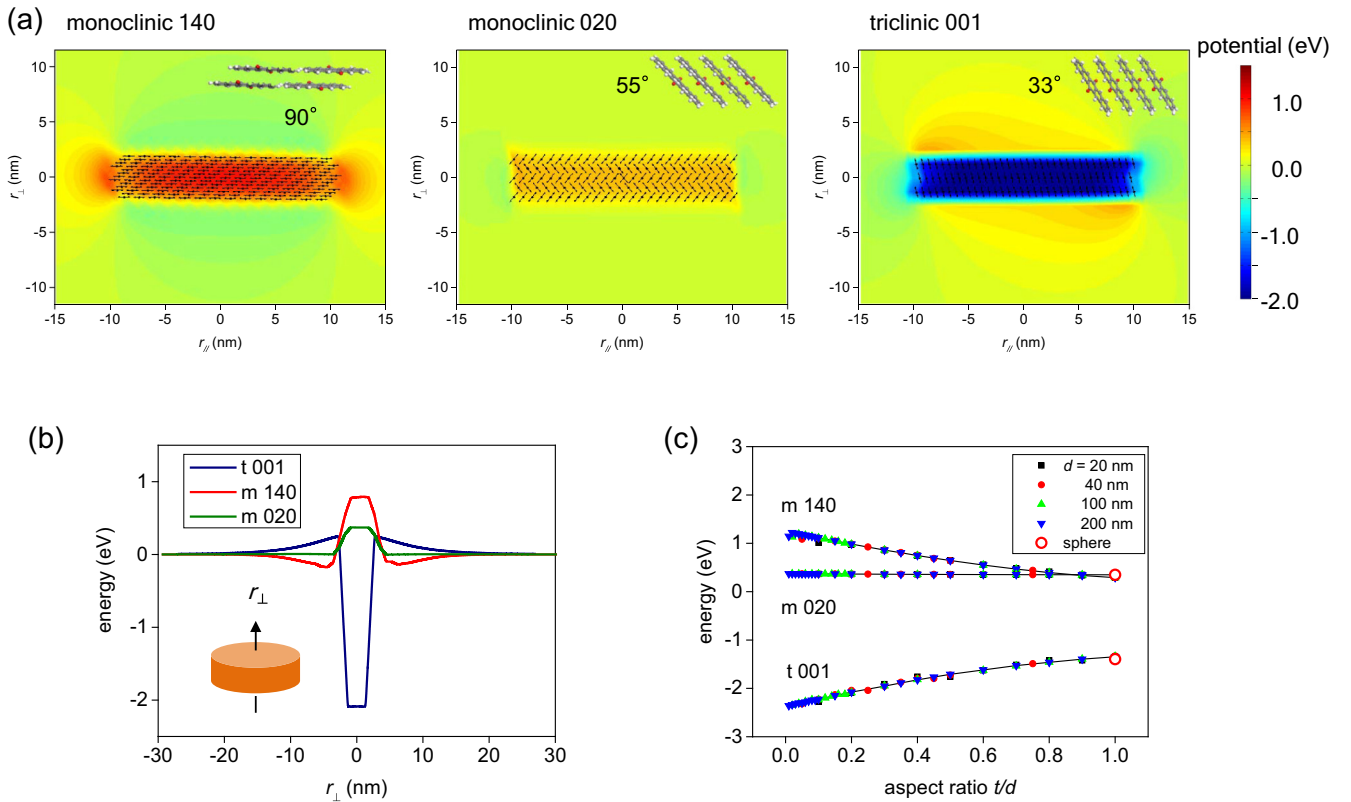


FIG. 4. The electrostatic potential generated by the quadrupole moments distributed at the molecular position in a disk cluster with the thickness of 4 nm and diameter of 20 nm. The calculation was made for the 140 and 020 surfaces of the monoclinic form (indicated by $m140$ and $m020$, respectively), and the 001 surface of the triclinic form ($t001$). (a) Potential maps. The arrows indicate the position of molecules and direction of quadrupole moments. (b) The potential as a function of distance from the center of the disk along the normal to the surface. (c) The potential energy at the center of disk clusters as a function of aspect ratio t/d and that of a spherical cluster with a radius d ranging from 20 to 200 nm.

(in a cluster with the 140 surface of the monoclinic form), 55° (the 020 surface of the monoclinic form), and 33° (the 001 surface of the triclinic form), respectively. These values are in qualitative agreement with the experimental results. Note that the positive U value for positive (negative) charge means the destabilization (stabilization) of the system and corresponds to the negative (positive) W .

Figure 4(b) shows the potential energy along the normal to the substrate surface. The energy in the cluster ($-2.5 \text{ nm} < r_{\perp} < 2.5 \text{ nm}$) is mostly uniform and different from that at the infinite distance as mentioned above. The potential energy near the surface outside the cluster ($2.5 \text{ nm} < r_{\perp} < 10 \text{ nm}$) also varies by -0.18 eV ($\theta_y = 90^\circ$), 0 eV (55°), and 0.25 eV (33°) meaning that the orientation dependence of the surface potential leads to variation of the vacuum level and hence of the ionization energy and electron affinity. The results indicate that the molecular quadrupole affects the ionization energy and electron affinity through the following two ways: (1) the electrostatic potential in the cluster (bulk effect) and (2) the shift of vacuum level (surface effect). In the PNQ films, the bulk effect (1) is larger than the surface effect (2).

Since the charge-permanent quadrupole interaction is a long-range interaction, the potential inside the cluster is affected by the macroscopic shape of the cluster [16,17]. Figure 4(c) shows the potential energy of the center of the disk cluster with various thicknesses t and diameters d (between 20

and 200 nm). It is found that the potential energy depends on only the aspect ratio t/d and converges to that of the spherical cluster which does not depend on the radius of the sphere. These results indicate that the sample shape is crucial to the electrostatic energy.

VI. CONCLUSION

We demonstrated that the electrostatic W and electronic polarization E_p energies of organic thin films can be determined based solely on experimental results of ultraviolet and low-energy inverse photoelectron spectroscopies. First, the polarization energies for positive P^+ and negative P^- charges are evaluated precisely from Eq. (1). Then, the polarization energies are decomposed into the induction E_p and electrostatic W terms based on the different response to the polarity of the charge [Eq. (3)]. This procedure was applied to the orientation-dependent energy levels of 6,13-pentacenequinone (PNQ) films with controlled molecular orientations on the same silicon oxide surface. It turns out that the electrostatic energy W predominantly depends on the molecular orientation. Since W is approximated by charge-permanent quadrupole interaction, the present results confirm the previous prediction that the electrostatic energy or the permanent-quadrupole moment of molecule is the origin of orientation-dependent

energy levels [16,20]. The results are also fully consistent with the first-principles calculation and the electrostatic energy of charge-permanent quadrupole interactions. The present work will stimulate further experimental and theoretical studies on a role of the electrostatic and electron polarization energies in organic semiconductors.

ACKNOWLEDGMENTS

The authors thank Prof. Itaru Osaka at Hiroshima University and Prof. Koji Okudaira at Chiba University for help with

GIXD and NEXAFS measurements, respectively. GIXD experiments were performed at the BL46XU of SPring-8 with the approval of the Japan Synchrotron Radiation Research Institute (JASRI) (Proposal No. 2014B1915). NEXAFS experiments were performed with the approval of the Photon Factory Program Advisory Committee (PF-PAC No. 2013G170). First-principles calculations were done by using the computational facilities in the Supercomputer Center, the Institute for Solid State Physics, and the Cyberscience Center, Tohoku University. This research was supported by JSPS KAKENHI Grants No. 25410093, No. 26288007, and No. 26105011.

The authors declare no competing financial interests.

-
- [1] J.-P. Yang, F. Bussolotti, S. Kera, and N. Ueno, *J. Phys. D: Appl. Phys.* **50**, 423002 (2017).
- [2] K. Akaike, *Jpn. J. Appl. Phys.* **57**, 03EA03 (2018).
- [3] K. Seki, Y. Harada, K. Ohno, and H. Inokuchi, *Bull. Chem. Soc. Jpn.* **47**, 1608 (1974).
- [4] F. Gutmann and L. E. Lyons, *Organic Semiconductors* (John Wiley and Sons, Inc., New York, Sydney, 1967).
- [5] N. Sato, K. Seki, and H. Inokuchi, *J. Chem. Soc., Faraday Trans. 2* **77**, 1621 (1981).
- [6] S. Hasegawa, T. Mori, K. Imaeda, S. Tanaka, Y. Yamashita, H. Inokuchi, H. Fujimoto, K. Seki, and N. Ueno, *J. Chem. Phys.* **100**, 6969 (1994).
- [7] H. Yamane, S. Kera, K. K. Okudaira, D. Yoshimura, K. Seki, and N. Ueno, *Phys. Rev. B* **68**, 033102 (2003).
- [8] N. Koch, A. Vollmer, I. Salzmänn, B. Nickel, H. Weiss, and J. P. Rabe, *Phys. Rev. Lett.* **96**, 156803 (2006).
- [9] N. Ueno and S. Kera, *Prog. Surf. Sci.* **83**, 490 (2008).
- [10] H. Yamane and N. Kosugi, *Phys. Rev. Lett.* **111**, 086602 (2013).
- [11] Y. Nakayama, Y. Mizuno, M. Hikasa, M. Yamamoto, M. Matsunami, S. Ideta, K. Tanaka, H. Ishii, and N. Ueno, *J. Phys. Chem. Lett.* **8**, 1259 (2017).
- [12] H. Yoshida, K. Yamada, J. Tsutsumi, and N. Sato, *Phys. Rev. B* **92**, 075145 (2015).
- [13] E. A. Silinsh and V. Čápek, *Organic Molecular Crystals: Interaction, Localization, and Transport Phenomena* (American Institute of Physics, New York, 1994).
- [14] P. J. Bounds and R. W. Munn, *Chem. Phys.* **59**, 41 (1981).
- [15] N. Sato, H. Inokuchi, and E. A. Silinsh, *Chem. Phys.* **115**, 269 (1987).
- [16] B. J. Topham and Z. G. Soos, *Phys. Rev. B* **84**, 165405 (2011).
- [17] C. Poelking, M. Tietze, C. Elschner, S. Olthof, D. Hertel, B. Baumeier, F. Würthner, K. Meerholz, K. Leo, and D. Andrienko, *Nat. Mater.* **14**, 434 (2015).
- [18] S. M. Ryno, C. Risko, and J.-L. Brédas, *ACS Appl. Mater. Interfaces* **8**, 14053 (2016).
- [19] S. Duhm, G. Heimel, I. Salzmänn, H. Glowatzki, R. L. Johnson, A. Vollmer, J. P. Rabe, and N. Koch, *Nat. Mater.* **7**, 326 (2008).
- [20] G. Heimel, I. Salzmänn, S. Duhm, and N. Koch, *Chem. Mater.* **23**, 359 (2011).
- [21] M. Schwarze, W. Tress, B. Beyer, F. Gao, R. Scholz, C. Poelking, K. Ortstein, A. A. Günther, D. Kasemann, D. Andrienko, and K. Leo, *Science* **352**, 1446 (2016).
- [22] N. Ueno, *Science* **352**, 1395 (2016).
- [23] C. Poelking and D. Andrienko, *J. Chem. Theory Comput.* **12**, 4516 (2016).
- [24] C. Poelking and D. Andrienko, *J. Am. Chem. Soc.* **137**, 6320 (2015).
- [25] G. D'Avino, L. Muccioli, F. Castet, C. Poelking, D. Andrienko, Z. G. Soos, J. Cornil, and D. Beljonne, *J. Phys.: Condens. Matter* **28**, 433002 (2016).
- [26] K. Nakano and K. Tajima, *Adv. Mater.* **29**, 1603269 (2017).
- [27] W. Chen, H. Huang, S. Chen, Y. L. Huang, X. Y. Gao, and A. T. S. Wee, *Chem. Mater.* **20**, 7017 (2008).
- [28] I. Salzmänn, S. Duhm, G. Heimel, M. Oehzelt, R. Kniprath, R. L. Johnson, J. P. Rabe, and N. Koch, *J. Am. Chem. Soc.* **130**, 12870 (2008).
- [29] W. Chen, S. Chen, S. Chen, Y. L. Huang, H. Huang, D. C. Qi, X. Y. Gao, J. Ma, and A. T. S. Wee, *J. Appl. Phys.* **106**, 064910 (2009).
- [30] W. Chen, D. C. Qi, Y. L. Huang, H. Huang, Y. Z. Wang, S. Chen, X. Y. Gao, and A. T. S. Wee, *J. Phys. Chem. C* **113**, 12832 (2009).
- [31] H. Huang, W. Chen, S. Chen, D. C. Qi, X. Y. Gao, and A. T. S. Wee, *Appl. Phys. Lett.* **94**, 163304 (2009).
- [32] S. Duhm, S. Hosoumi, I. Salzmänn, A. Gerlach, M. Oehzelt, B. Wedl, T.-L. Lee, F. Schreiber, N. Koch, N. Ueno, and S. Kera, *Phys. Rev. B* **81**, 045418 (2010).
- [33] H. Y. Mao, R. Wang, H. Huang, Y. Z. Wang, X. Y. Gao, S. N. Bao, A. T. S. Wee, and W. Chen, *J. Appl. Phys.* **108**, 053706 (2010).
- [34] W. Chen, D. C. Qi, H. Huang, X. Y. Gao, and A. T. S. Wee, *Adv. Funct. Mater.* **21**, 410 (2011).
- [35] C. Wang, A. J. Turinske, and Y. Gao, *Appl. Phys. B: Lasers Opt.* **113**, 361 (2013).
- [36] W. N. Han, K. Yonezawa, R. Makino, K. Kato, A. Hinderhofer, R. Murdey, R. Shiraishi, H. Yoshida, N. Sato, N. Ueno, and S. Kera, *Appl. Phys. Lett.* **103**, 253301 (2013).
- [37] O. T. Hofmann, H. Glowatzki, C. Bürker, G. M. Rangger, B. Bröker, J. Niederhausen, T. Hosokai, I. Salzmänn, R.-P. Blum, R. Rieger, A. Vollmer, P. Rajput, A. Gerlach, K. Müllen, F. Schreiber, E. Zojer, N. Koch, and S. Duhm, *J. Phys. Chem. C* **121**, 24657 (2017).
- [38] N. A. Ran, S. Roland, J. A. Love, V. Savikhin, C. J. Takacs, Y.-T. Fu, H. Li, V. Coropceanu, X. Liu, J.-L. Brédas, G. C. Bazan, M. F. Toney, D. Neher, and T.-Q. Nguyen, *Nat. Commun.* **8**, 79 (2017).
- [39] H. Yoshida, *Chem. Phys. Lett.* **539-540**, 180 (2012).
- [40] H. Yoshida, *Anal. Bioanal. Chem.* **406**, 2231 (2014).

- [41] H. Yoshida, *J. Electron Spectrosc. Relat. Phenom.* **204**, 116 (2015).
- [42] S. Fabiano, H. Yoshida, Z. Chen, A. Facchetti, and M. A. Loi, *ACS Appl. Mater. Interfaces* **5**, 4417 (2013).
- [43] W. Han, H. Yoshida, N. Ueno, and S. Kera, *Appl. Phys. Lett.* **103**, 123303 (2013).
- [44] Y. Ie, M. Karakawa, S. Jinnai, H. Yoshida, A. Saeki, S. Seki, S. Yamamoto, H. Ohkita, and Y. Aso, *Chem. Commun.* **50**, 4123 (2014).
- [45] H. Yoshida, *J. Phys. Chem. C* **118**, 24377 (2014).
- [46] H. Yoshida and K. Yoshizaki, *Org. Electron.* **20**, 24 (2015).
- [47] H. Yoshida, *J. Phys. Chem. C* **119**, 24459 (2015).
- [48] M. Saito, I. Osaka, Y. Suda, H. Yoshida, and K. Takimiya, *Adv. Mater.* **28**, 6921 (2016).
- [49] K. Kawashima, T. Fukuhara, Y. Suda, Y. Suzuki, T. Koganezawa, H. Yoshida, H. Ohkita, I. Osaka, and K. Takimiya, *J. Am. Chem. Soc.* **138**, 10265 (2016).
- [50] S. Jinnai, Y. Ie, Y. Kashimoto, H. Yoshida, M. Kawakawa, and Y. Aso, *J. Mater. Chem. A* **5**, 3932 (2017).
- [51] Y. Zhong, S. Izawa, K. Hashimoto, K. Tajima, T. Koganezawa, and H. Yoshida, *J. Phys. Chem. C* **119**, 23 (2015).
- [52] W. H. Lee, J. Park, S. H. Sim, S. Lim, K. S. Kim, B. H. Hong, and K. Cho, *J. Am. Chem. Soc.* **133**, 4447 (2011).
- [53] H. Yoshida, *Rev. Sci. Instrum.* **85**, 016101 (2014).
- [54] M. J. Frisch, G. W. Trucks, H. B. Schlegel, G. E. Scuseria, M. A. Robb, J. R. Cheeseman, G. Scalmani, V. Barone, B. Mennucci, G. A. Petersson, H. Nakatsuji, M. Caricato, X. Li, H. P. Hratchian, A. F. Izmaylov, J. Bloino, G. Zheng, J. L. Sonnenberg, M. Hada, M. Ehara *et al.*, GAUSSIAN09, Revision A.02 (Gaussian, Inc., Wallingford CT, 2013).
- [55] The quadrupole tensor \mathbf{Q} calculated at the B3LYP/6-311 + G(d,p) level has principle components of $Q_{xx} = -8.3 \times 10^{-39} \text{ C m}^2$ (along the molecular short axis), $Q_{yy} = 16.9 \times 10^{-39} \text{ C m}^2$ (along the molecular long axis), and $Q_{zz} = -8.6 \times 10^{-39} \text{ C m}^2$ (along the normal to the plane) [77]. The largest component Q_{yy} is twice as large as another component Q_{xx} or Q_{zz} being almost the same as each other. Such a quadrupole is modeled as a linear array of three point charges as shown in Fig. 1(a) where the components of the tensor are $Q_{yy} = +4lq^2$ and $Q_{xx} = Q_{zz} = -2lq^2$.
- [56] See Supplemental Material at <http://link.aps.org/supplemental/10.1103/PhysRevB.97.245206> for NEXAFS and FT-IR data; GIXD and NEXAFS results of PNQ on HOPG; photon energy dependence of LEIPS spectra and the determination of electron affinities; thickness dependence of LEIPS spectra; and the detailed description of the first-principles calculations (see also Refs. [78–90]).
- [57] D. K. Hwang, K. Kim, J. H. Kim, S. Im, D.-Y. Jung, and E. Kim, *Appl. Phys. Lett.* **85**, 5568 (2004).
- [58] P. Parris, S. Picozzi, and L. Ottaviano, *Org. Electron.* **8**, 498 (2007).
- [59] I. Salzmann, R. Opitz, S. Rogaschewski, J. P. Rabe, N. Koch, and B. Nickel, *Phys. Rev. B* **75**, 174108 (2007).
- [60] I. Salzmann, D. Nabok, M. Oehzelt, S. Duhm, A. Moser, G. Heimel, P. Puschnig, C. Ambrosch-Draxl, J. P. Rabe, and N. Koch, *Cryst. Growth Des.* **11**, 600 (2011).
- [61] H. Yamane, S. Nagamatsu, H. Fukagawa, S. Kera, R. Friedlein, K. K. Okudaira, and N. Ueno, *Phys. Rev. B* **72**, 153412 (2005).
- [62] H. Fukagawa, S. Kera, T. Kataoka, S. Hosoumi, Y. Watanabe, K. Kudo, and N. Ueno, *Adv. Mater.* **19**, 665 (2007).
- [63] I. Salzmann, A. Moser, M. Oehzelt, T. Breuer, X. Feng, Z.-Y. Juang, D. Nabok, R. G. Della Valle, S. Duhm, G. Heimel, A. Brillante, E. Venuti, I. Bilotti, C. Christodoulou, J. Frisch, P. Puschnig, C. Draxl, G. Witte, K. Müllen, and N. Koch, *ACS Nano* **6**, 10874 (2012).
- [64] S. Kera, S. Hosoumi, K. Sato, H. Fukagawa, S. Nagamatsu, Y. Sakamoto, T. Suzuki, H. Huang, W. Chen, A. T. S. Wee, V. Coropceanu, and N. Ueno, *J. Phys. Chem. C* **117**, 22428 (2013).
- [65] W. R. Salaneck, *Phys. Rev. Lett.* **40**, 60 (1978).
- [66] Y. Harada, H. Ozaki, and K. Ohno, *Phys. Rev. Lett.* **52**, 2269 (1984).
- [67] H. Yoshida, E. Ito, M. Hara, and N. Sato, *Synth. Met.* **161**, 2549 (2012).
- [68] H. Yoshida and N. Sato, *J. Phys. Chem. C* **116**, 10033 (2012).
- [69] G. Heimel, S. Duhm, I. Salzmann, A. Gerlach, A. Strozecka, J. Niederhausen, C. Bürker, T. Hosokai, I. Fernandez-Torrente, G. Schulze, S. Winkler, A. Wilke, R. Schlesinger, J. Frisch, B. Bröker, A. Vollmer, B. Detlefs, J. Pflaum, S. Kera, K. J. Franke *et al.*, *Nat. Chem.* **5**, 187 (2013).
- [70] T. Masubuchi, Y. Sugawara, and A. Nakajima, *J. Chem. Phys.* **145**, 244306 (2016).
- [71] W. Kohn, *Phys. Rev. Lett.* **76**, 3168 (1996).
- [72] D. Deutsch, A. Natan, Y. Shapira, and L. Kronik, *J. Am. Chem. Soc.* **129**, 2989 (2007).
- [73] L. Hedin, *Phys. Rev.* **139**, A796 (1965).
- [74] M. M. Rieger, L. Steinbeck, I. D. White, H. N. Rojas, and R. W. Godby, *Comput. Phys. Commun.* **117**, 211 (1999).
- [75] L. Steinbeck, A. Rubio, L. Reining, M. Torrent, I. D. White, and R. W. Godby, *Comput. Phys. Commun.* **125**, 105 (2000).
- [76] C. Freysoldt, P. Eggert, P. Rinke, A. Schindlmayr, R. W. Godby, and M. Scheffler, *Comput. Phys. Commun.* **176**, 1 (2007).
- [77] D. Käfer, M. E. Helou, C. Gemel, and G. Witte, *Cryst. Growth Des.* **8**, 3053 (2008).
- [78] J. Stöhr, *NEXAFS Spectroscopy* (Springer, Heidelberg, 1992).
- [79] Y. Morikawa, H. Ishii, and K. Seki, *Phys. Rev. B* **69**, 041403 (2004).
- [80] A. V. Dzyabchenko, V. E. Zavodnik, and V. K. Belsky, *Acta Crystallogr. Sect. B* **35**, 2250 (1979).
- [81] M. Otani and O. Sugino, *Phys. Rev. B* **73**, 115407 (2006).
- [82] I. Hamada, M. Otani, O. Sugino, and Y. Morikawa, *Phys. Rev. B* **80**, 165411 (2009).
- [83] N. Troullier and J. L. Martins, *Phys. Rev. B* **43**, 1993 (1991).
- [84] S. Grimme, *J. Comput. Chem.* **27**, 1787 (2006).
- [85] A. Schindlmayr, *Phys. Rev. B* **87**, 075104 (2013).
- [86] J. Heyd, G. E. Scuseria, and M. Ernzerhof, *J. Chem. Phys.* **118**, 8207 (2003).
- [87] J. Heyd, G. E. Scuseria, and M. Ernzerhof, *J. Chem. Phys.* **124**, 219906 (2006).
- [88] A. V. Krukau, O. A. Vydrov, A. F. Izmaylov, and G. E. Scuseria, *J. Chem. Phys.* **125**, 224106 (2006).
- [89] S. Sharifzadeh, A. Biller, L. Kronik, and J. B. Neaton, *Phys. Rev. B* **85**, 125307 (2012).
- [90] S. Refaely-Abramson, S. Sharifzadeh, M. Jain, R. Baer, J. B. Neaton, and L. Kronik, *Phys. Rev. B* **88**, 081204(R) (2013).